Supplemental Material for:

Targeted gene therapy alleviates epilepsy and hyperexcitability in models of *SCN2A* deficiency

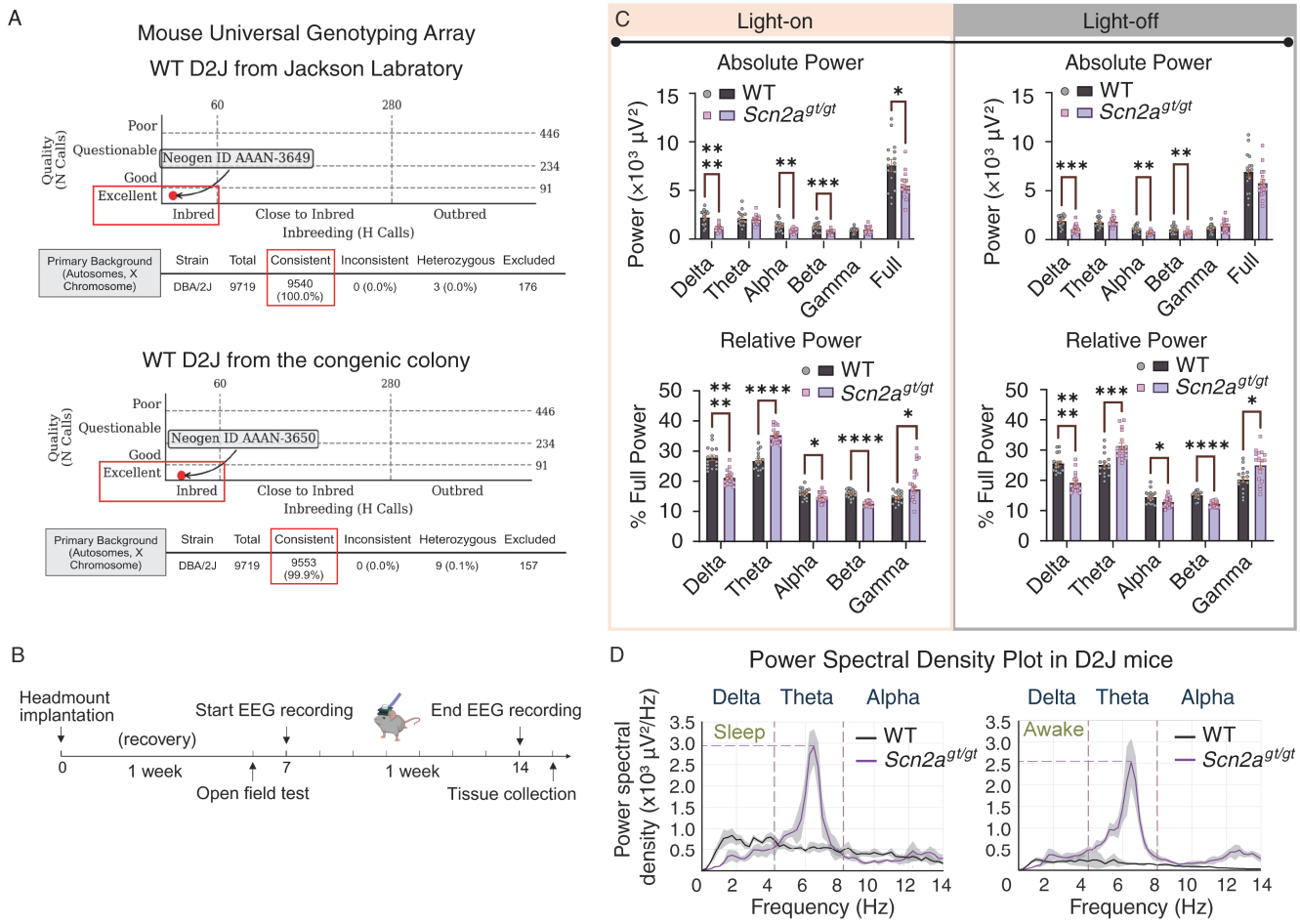
Zaiyang Zhang,[1,2,3&] Jingliang Zhang,[1,2&] Xiaoling Chen,[1,2&] Brody A. Deming,[1,2] Shivam Kant,[1,2] Purba Mandal,[1,2] Harish Kothandaraman,[4] Phillip J. SanMiguel,[5] Manasi S. Halurkar,[1,2] Akila D. Abeyaratna,[1,2] Morgan J. Robinson,[1,2,6] Iuliia Vitko,[7] Ronald P. Gaykema,[7] Chongli Yuan,[2,6] Nadia A. Lanman,[4,8] Matthew T. Tegtmeyer,[2,9] Dan Wang,[10] Guangping Gao,[10] Riyi Shi,[2,3] Edward Perez-Reyes,[7] and Yang Yang[1,2,4*]

[1]Borch Department of Medicinal Chemistry and Molecular Pharmacology, College of Pharmacy, Purdue University, West Lafayette, Indiana, USA; [2]Purdue Institute for Integrative Neuroscience, Purdue University, West Lafayette, Indiana, USA; [3]Department of Basic Medical Sciences, College of Veterinary Medicine, Purdue University, West Lafayette, Indiana, USA; [4]Purdue Institute for Cancer Research, Purdue University, West Lafayette, Indiana, USA; [5]Purdue Genomics Core, Bindley Bioscience Center, Purdue University, West Lafayette, Indiana, USA; [6]Davidson School of Chemical Engineering, Purdue University, West Lafayette, Indiana, USA; [7]University of Virginia School of Medicine, Charlottesville, Virginia, USA; [8]Department of Comparative Pathobiology, College of Veterinary Medicine, Purdue University, West Lafayette, Indiana, USA; [9]Department of Biological Sciences, College of Science, Purdue University, West Lafayette, Indiana, USA; [10]Department of Genetic and Cellular Medicine, University of Massachusetts Chan Medical School, Worcester, Massachusetts, USA;
[&]these authors contributed equally to this work.

*To whom correspondence should be addressed: Yang Yang (yangyang@purdue.edu)

Supplemental Material

Supplemental Figure 1



Supplemental Figure 1. D2J *Scn2a*$^{gt/gt}$ mice exhibit altered EEG spectral activity across light–dark and sleep–wake states.

(A) GigaMUGA analysis showing 99.9% genomic consistency between D2J congenic mice and WT D2J mice from Jackson Laboratory.

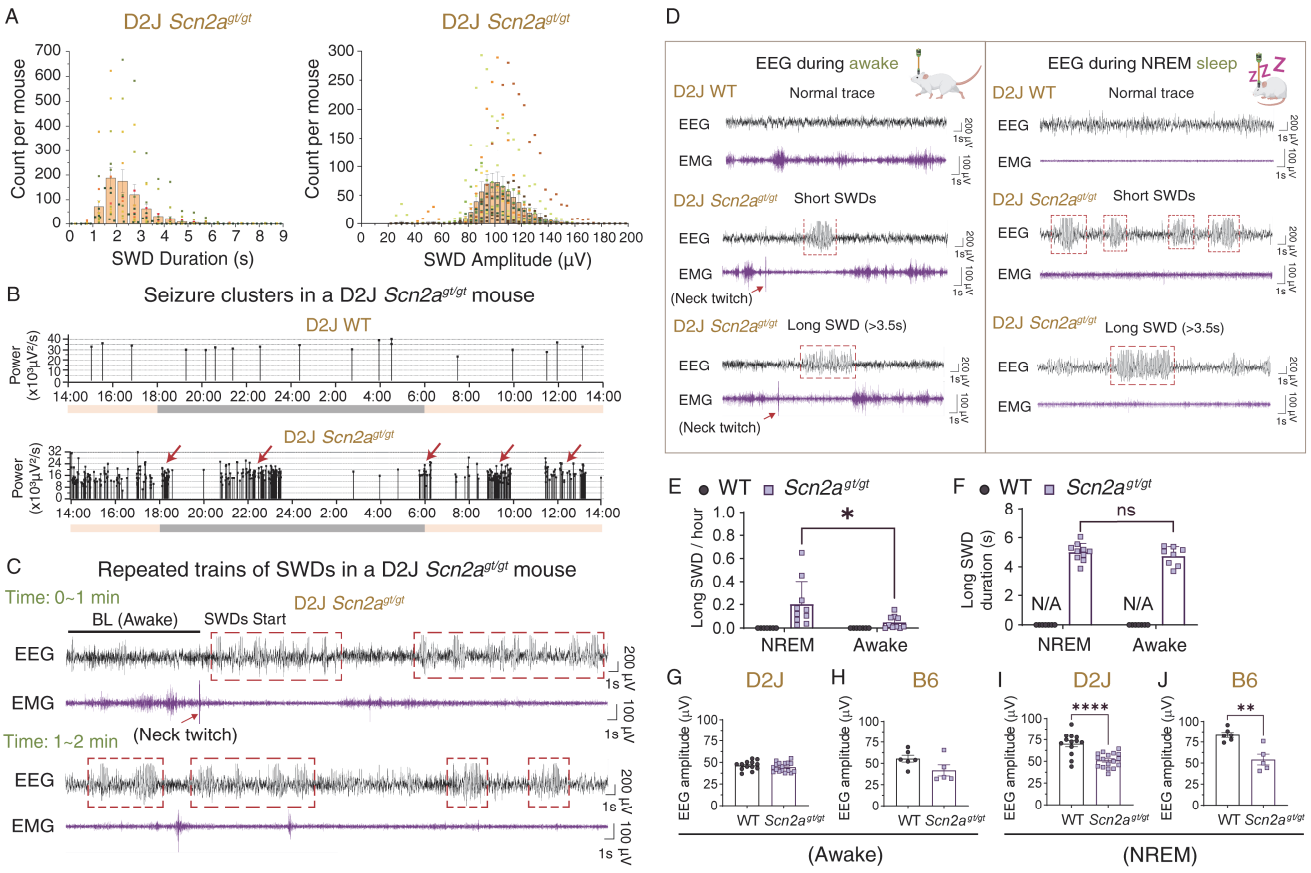
(B) Timeline of EEG recording. After surgery, mice recovered in their home cage for at least 1 week before 1 week of video-EEG monitoring.

(C) Absolute and relative EEG power distribution in D2J WT and D2J *Scn2a*$^{gt/gt}$ mice across 1 week of recording. Relative power was calculated by normalizing each frequency band to the total power for each animal. P values were calculated using multiple unpaired t tests with Holm-Šídák correction.

(D) Representative power spectral density plots comparing D2J WT and D2J *Scn2a*$^{gt/gt}$ mice during sleep and wake states. *Scn2a*$^{gt/gt}$ mice show increased power density in the theta range (4–8 Hz), corresponding to the SWD frequency band, with higher theta-band power during sleep than wakefulness.

Data are presented as mean ± SEM. **P* < 0.05; ***P* < 0.01; ****P* < 0.001; *****P* < 0.0001.

Supplemental Figure 2



Supplemental Figure 2. SWDs cluster temporally and occur more frequently during NREM sleep in D2J *Scn2a*$^{gt/gt}$ mice.

(A) Distribution of SWD duration (s) (left) and peak-to-peak amplitude (μV) (right) in D2J *Scn2a*$^{gt/gt}$ mice, binned per mouse at 0.5 s and 4 μV. Bars show mean counts per bin ± SEM; colored points represent individual mice. Gaussian fits yielded centers of approximately 2.1 s and 101.9 μV, respectively.

(B) Representative images show frequent SWDs in D2J *Scn2a*$^{gt/gt}$ mice clustered within specific 24-hour windows, whereas D2J WT mice have fewer SWDs distributed throughout the day. Beige indicates lights on; grey indicates lights off.

(C) EEG2 and EMG recording of a D2J *Scn2a*$^{gt/gt}$ mouse showing repeated SWD trains lasting about 2 minutes. EMG shows a characteristic 'neck twitch' at onset. Red dashed boxes mark consecutive mature and immature SWDs.

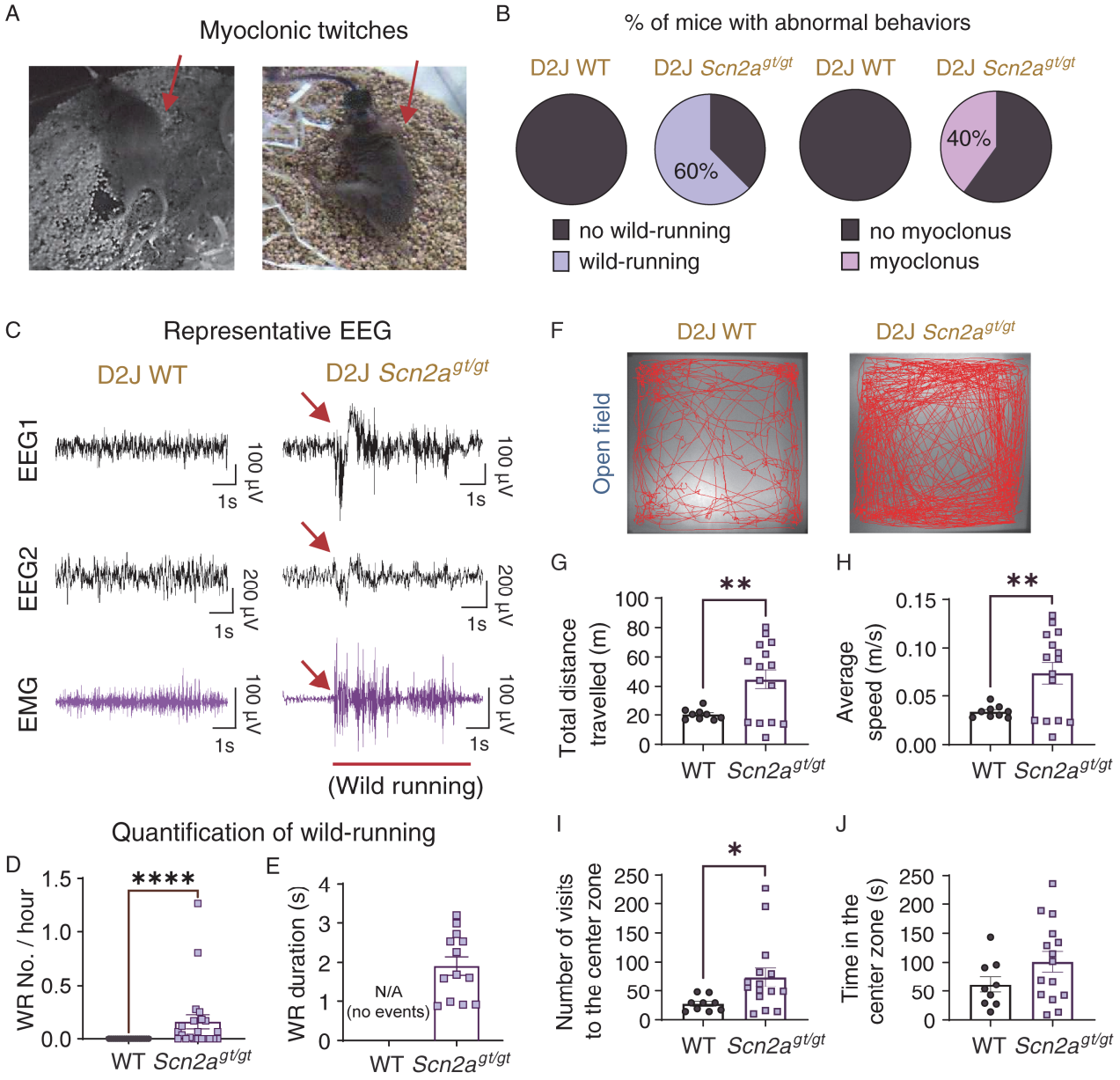
(D) Representative EEG and nuchal EMG traces from D2J WT and D2J *Scn2a*$^{gt/gt}$ mice during wakefulness (left) and NREM sleep (right). Neck twitches preceding SWDs during wakefulness were detected by EMG and confirmed by video (not shown).

(E and F) Frequency and duration of long SWDs (>3.5 s) in D2J WT and D2J *Scn2a*$^{gt/gt}$ mice during NREM sleep and wakefulness. In D2J *Scn2a*$^{gt/gt}$ mice, long SWDs were less frequent during wakefulness, whereas duration did not differ significantly between states. Statistical comparisons used two-way ANOVA with Šídák's multiple-comparisons test.

(G-J) EEG baseline amplitude outside SWDs in D2J and B6 mice. In both strains, *Scn2a*$^{gt/gt}$ mice had lower amplitude during NREM sleep but not wakefulness compared with WT littermates. Comparisons used an unpaired Student's t-test or Mann–Whitney U test.

Data are presented as mean ± SEM. *P < 0.05; **P < 0.01; ***P < 0.001; ****P < 0.0001.

Supplemental Figure 3



Supplemental Figure 3. Absence seizure-associated behaviors and open-field hyperactivity in D2J *Scn2a*$^{gt/gt}$ mice.

(A) Video screenshots showing abnormal seizure-associated behaviors in two D2J *Scn2a*$^{gt/gt}$ mice.

(B) Percentage of D2J WT and *Scn2a*$^{gt/gt}$ mice exhibiting wild-running (WR) or myoclonic twitches.

(C) Representative EEG1, EEG2, and EMG traces from a walking D2J WT mouse and a D2J *Scn2a*$^{gt/gt}$ mouse during a wild-running episode. Red arrows indicate wild-running onset. Cortical EEG during wild running lacked a characteristic ictal pattern.

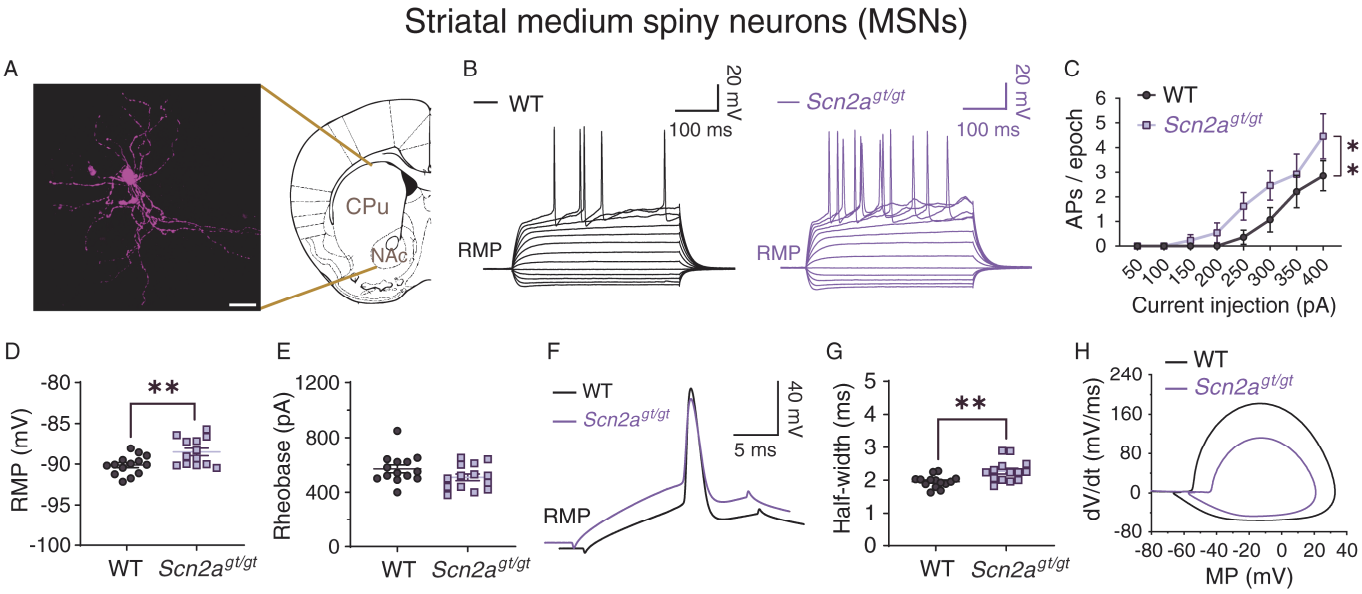
(D and E) Quantification of wild-running frequency and duration in D2J WT and D2J *Scn2a*$^{gt/gt}$ mice.

(F-J) Representative open-field tracking plots and locomotor activity. D2J *Scn2a*$^{gt/gt}$ mice traveled greater distances and moved faster than WT controls, with increased center-zone visits but no significant change in time spent in the center zone.

P values were calculated using an unpaired t-test or Mann-Whitney test.

Data are presented as mean ± SEM. **P* < 0.05; ***P* < 0.01; ****P* < 0.001; *****P* < 0.0001.

Supplemental Figure 4



Supplemental Figure 4. Striatal MSNs of D2J *Scn2a*$^{gt/gt}$ mice exhibit increased firing and altered AP waveforms.

(A) Representative neurobiotin-filled striatal medium spiny neuron (MSN) after whole-cell patch-clamp recording. Atlas schematic indicates the striatal recording region. Scale bars: 20 µm.

(B) Representative current-clamp recordings from D2J WT and *Scn2a*$^{gt/gt}$ MSNs at resting membrane potential (RMP). Neurons received 400-ms steps from −200 to +400 pA; steps from +50 to +400 pA were used to assess action potential (AP) firing.

(C) D2J *Scn2a*$^{gt/gt}$ MSNs fired more APs than WT MSNs during current steps.

(D) RMP was significantly more depolarized in D2J *Scn2a*$^{gt/gt}$ than in WT MSNs.

(E) Rheobase did not differ significantly between genotypes in MSNs.

(F) Representative single-AP waveforms from D2J WT and *Scn2a*$^{gt/gt}$ MSNs.

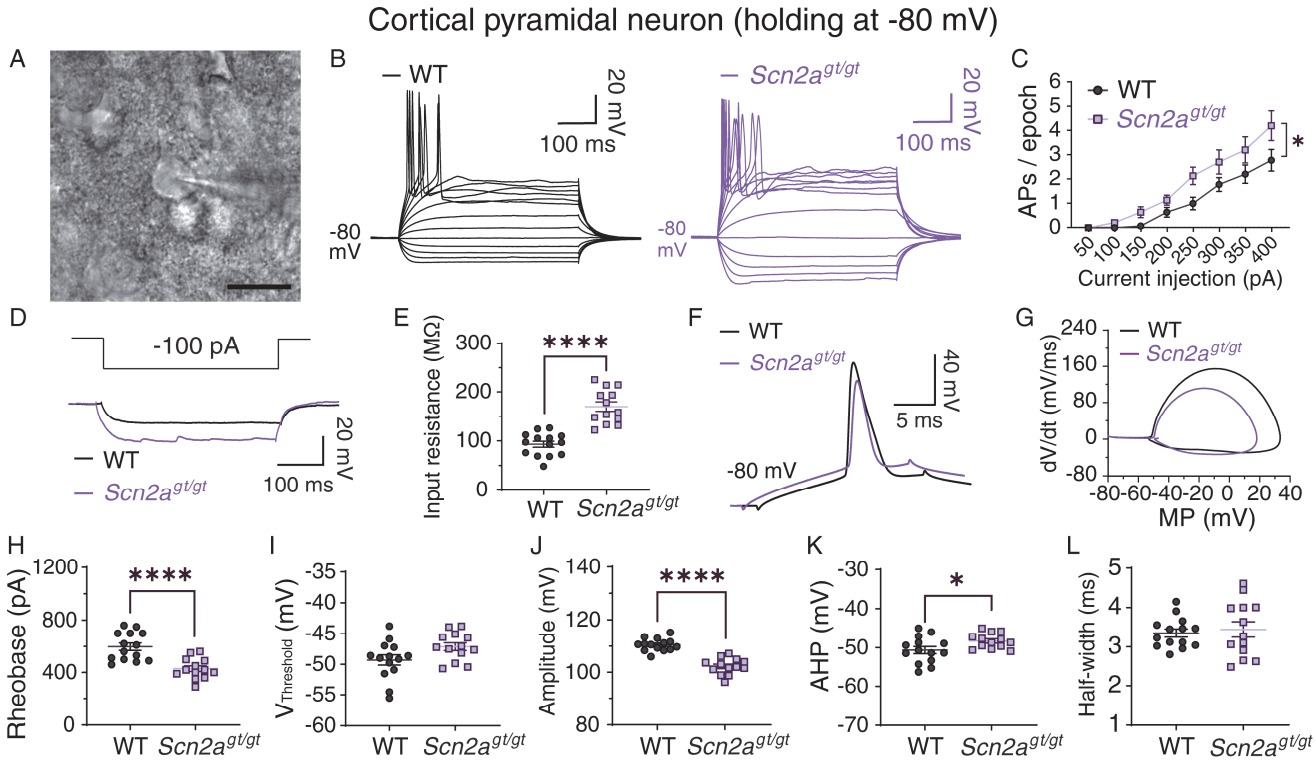
(G) AP half-width was significantly increased in D2J *Scn2a*$^{gt/gt}$ MSNs.

(H) Representative phase-plane plots showing altered AP waveforms in D2J *Scn2a*$^{gt/gt}$ versus WT MSNs.

Data are presented as mean ± SEM. **P* < 0.05; ***P* < 0.01; ****P* < 0.001; *****P* < 0.0001. n = 14 neurons from 4 WT mice and n = 13 neurons from 5 *Scn2a*$^{gt/gt}$ mice.

Statistical analyses: ordinary two-way ANOVA (C). Unpaired Student's t-test was used for all other comparisons.

Supplemental Figure 5



Supplemental Figure 5. Cortical neurons from D2J *Scn2a*$^{gt/gt}$ mice show increased firing when held at −80 mV.

(A) Representative image of a layer II/III cortical pyramidal neuron during whole-cell patch-clamp recording. Scale bar: 20 μm.

(B) Representative current-clamp traces from D2J WT and *Scn2a*$^{gt/gt}$ pyramidal neurons held at −80 mV during a series of hyperpolarizing and depolarizing current steps.

(C) Input–output relationships showing the number of action potentials (APs) evoked by increasing depolarizing current injections. *Scn2a*$^{gt/gt}$ neurons exhibited increased repetitive firing relative to WT neurons.

(D) Representative voltage responses to a −100 pA current injection used to assess passive membrane properties.

(E) Quantification of input resistance, which was increased in *Scn2a*$^{gt/gt}$ pyramidal neurons.

(F) Representative single-AP waveforms from WT and *Scn2a*$^{gt/gt}$ neurons.

(G) Representative phase-plane plots of the AP waveform (dV/dt versus membrane potential).

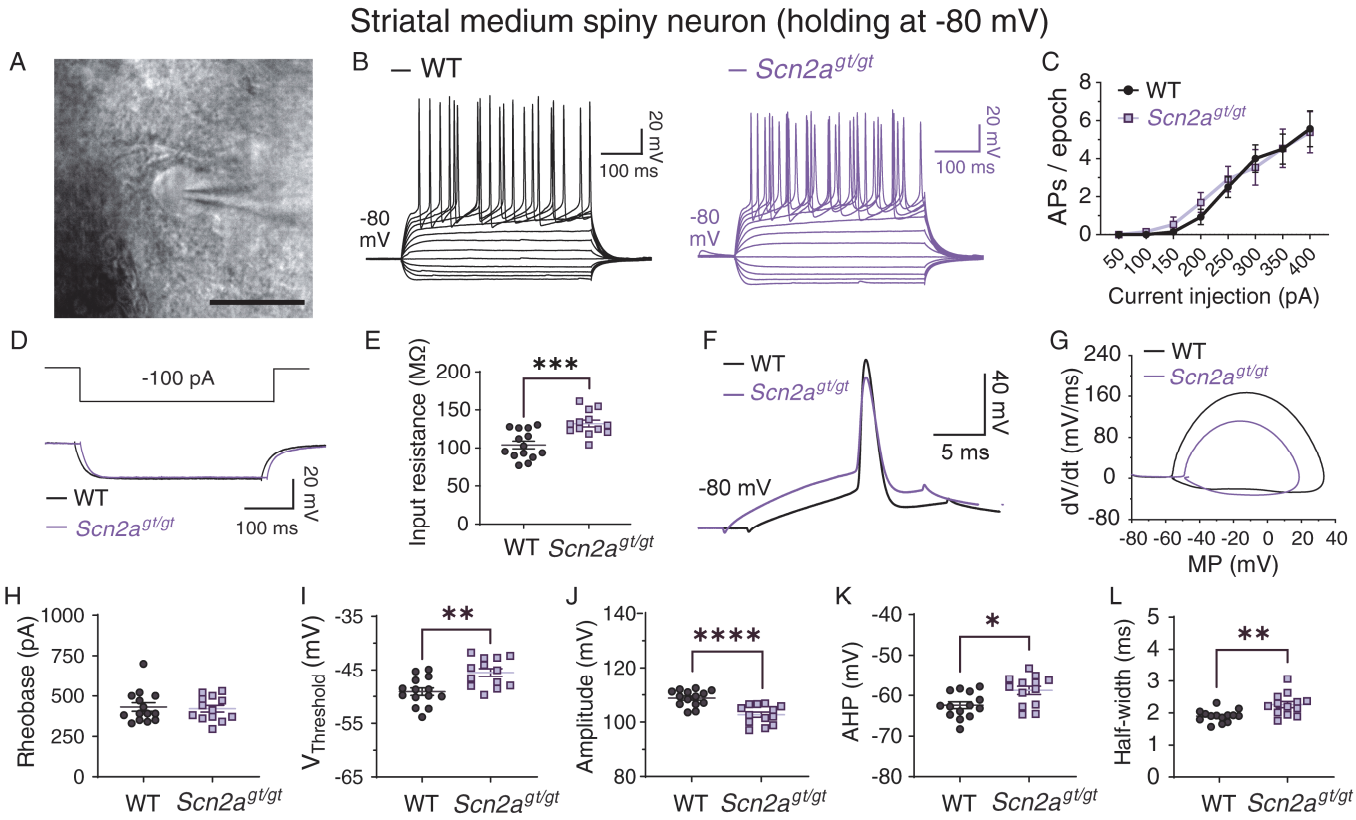
(H–L) Quantification of rheobase (H), AP voltage threshold (I), AP amplitude (J), fast afterhyperpolarization (AHP; K), and AP half-width (L).

Data are presented as mean ± SEM. **P* < 0.05; ***P* < 0.01; ****P* < 0.001; *****P* < 0.0001.

n = 14 neurons from 4 WT mice and n = 13 neurons from 5 *Scn2a*$^{gt/gt}$ mice.

Statistical significance was assessed by two-way ANOVA with Šídák's multiple-comparisons test for the input–output relationship and by unpaired two-tailed Student's t tests for other comparisons.

Supplemental Figure 6



Supplemental Figure 6. Increased firing in D2J *Scn2a*$^{gt/gt}$ MSNs was abolished when the neurons were held at −80 mV.

(A) Representative image of the morphology of a striatal MSN during whole-cell patch-clamp recording. Scale bar: 20 µm.

(B) Representative current-clamp traces from D2J WT and *Scn2a*$^{gt/gt}$ striatal MSNs held at −80 mV during a series of hyperpolarizing and depolarizing current steps.

(C) Input–output relationships showing the number of action potentials (APs) evoked by increasing depolarizing current injections.

(D) Representative voltage responses to a −100-pA current injection used to assess passive membrane properties.

(E) Quantification of input resistance, which was increased in *Scn2a*$^{gt/gt}$ striatal MSNs.

(F) Representative single-AP waveforms from WT and *Scn2a*$^{gt/gt}$ striatal MSNs.

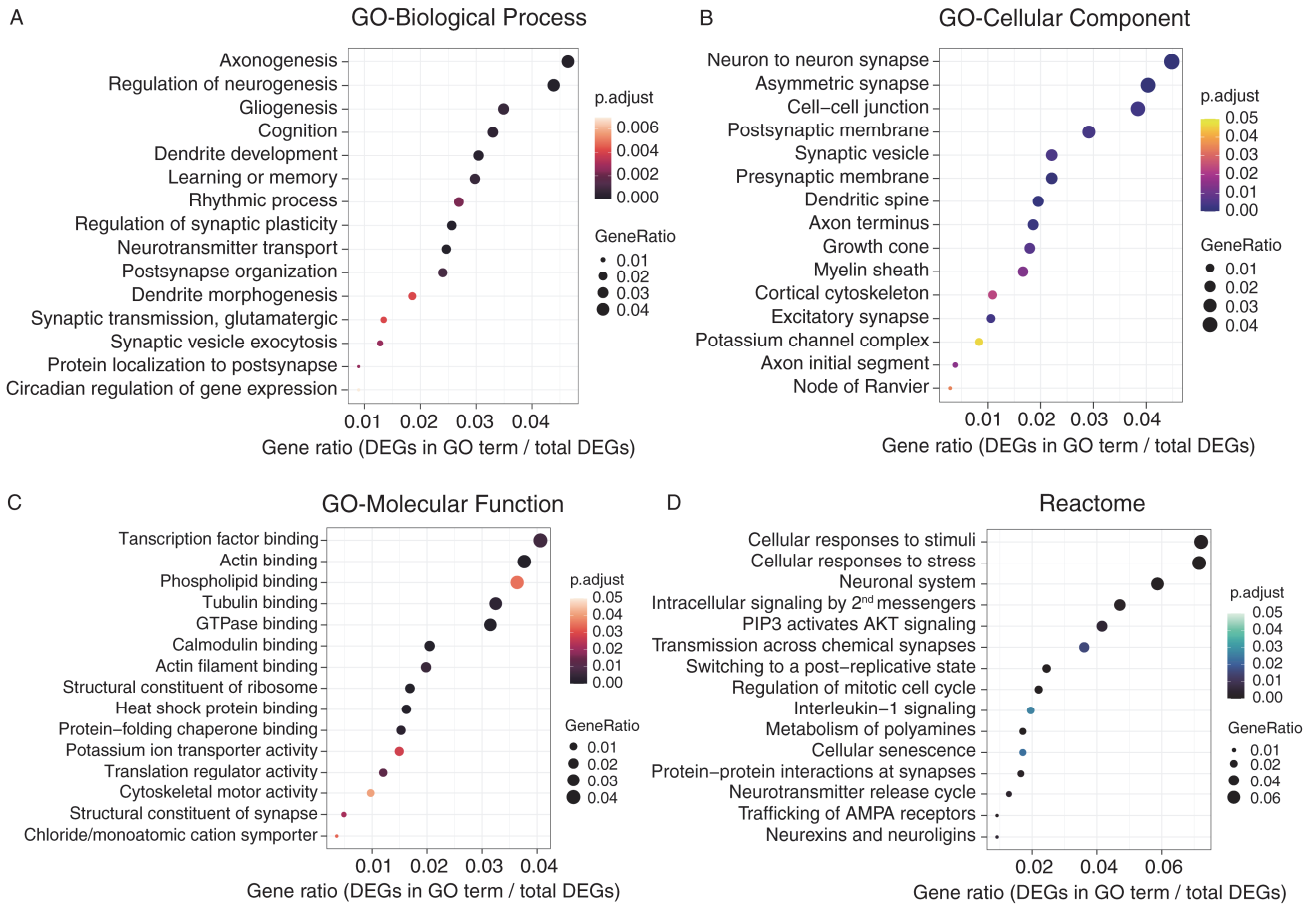
(G) Representative phase-plane plots of the AP waveform (dV/dt versus membrane potential).

(H–L) Quantification of rheobase (H), AP voltage threshold (I), AP amplitude (J), fast afterhyperpolarization (AHP; K), and AP half-width (L).

Data are presented as mean ± SEM. **P* < 0.05; ***P* < 0.01; ****P* < 0.001; *****P* < 0.0001. n = 14 neurons from 4 WT mice and n = 13 neurons from 5 Scn2agt/gt mice.

Statistical significance was assessed by two-way ANOVA with Šídák's multiple-comparisons test for the input–output relationship and by unpaired two-tailed Student's t tests for other comparisons.

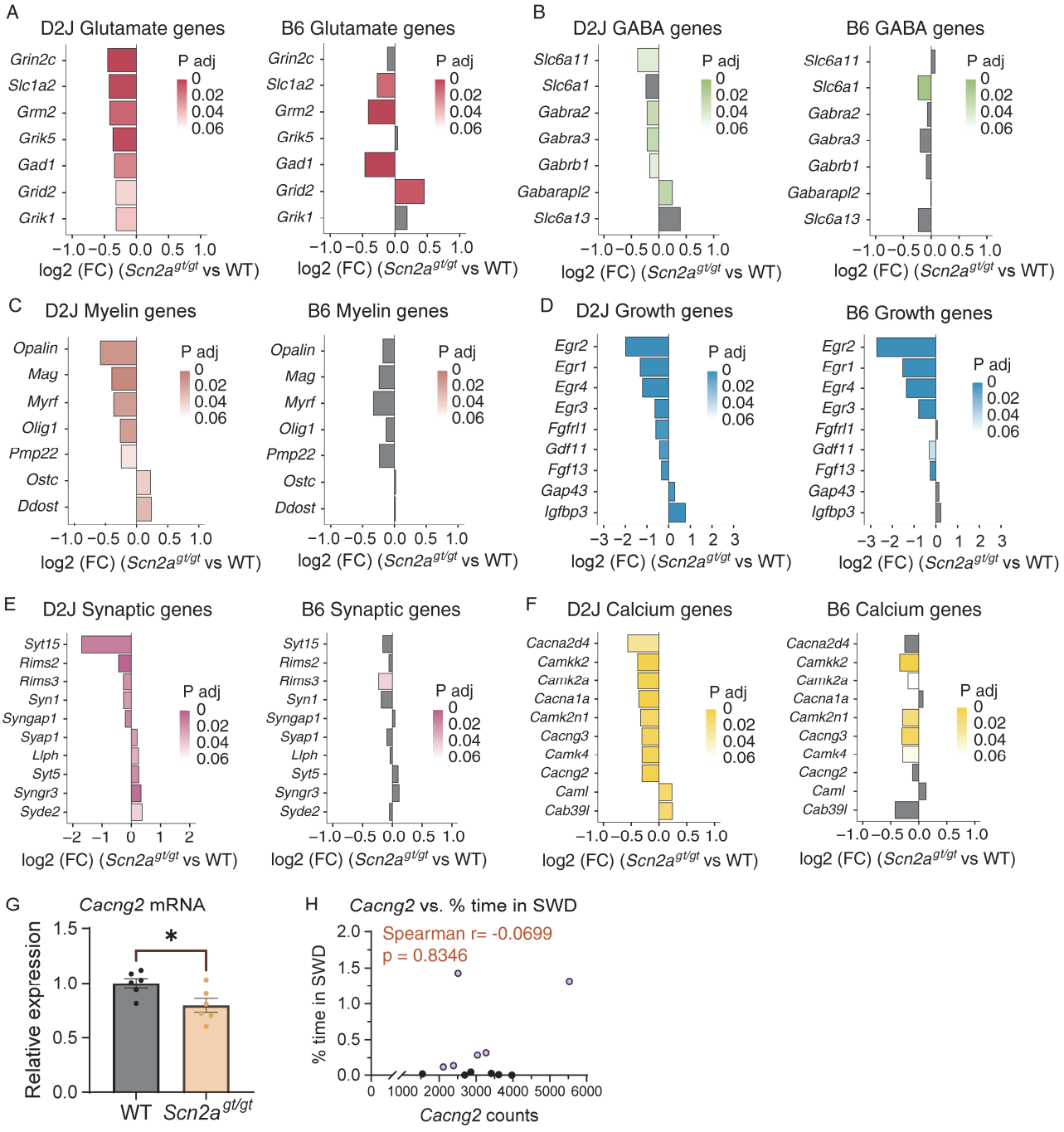
Supplemental Figure 7



Supplemental Figure 7. Gene Ontology (GO) and Reactome enrichment analyses highlight neurodevelopmental, synaptic, and potassium channel processes in D2J *Scn2a*$^{gt/gt}$ mice.

(A–D) Enrichment analyses of cortical DEGs in D2J *Scn2a*$^{gt/gt}$ versus WT mice: GO biological process (A), GO cellular component (B), GO molecular function (C), and Reactome pathways (D).

Supplemental Figure 8



Supplemental Figure 8. Cross-strain analysis of gene-expression changes in the cortex of D2J and B6 *Scn2a*$^{gt/gt}$ mice.

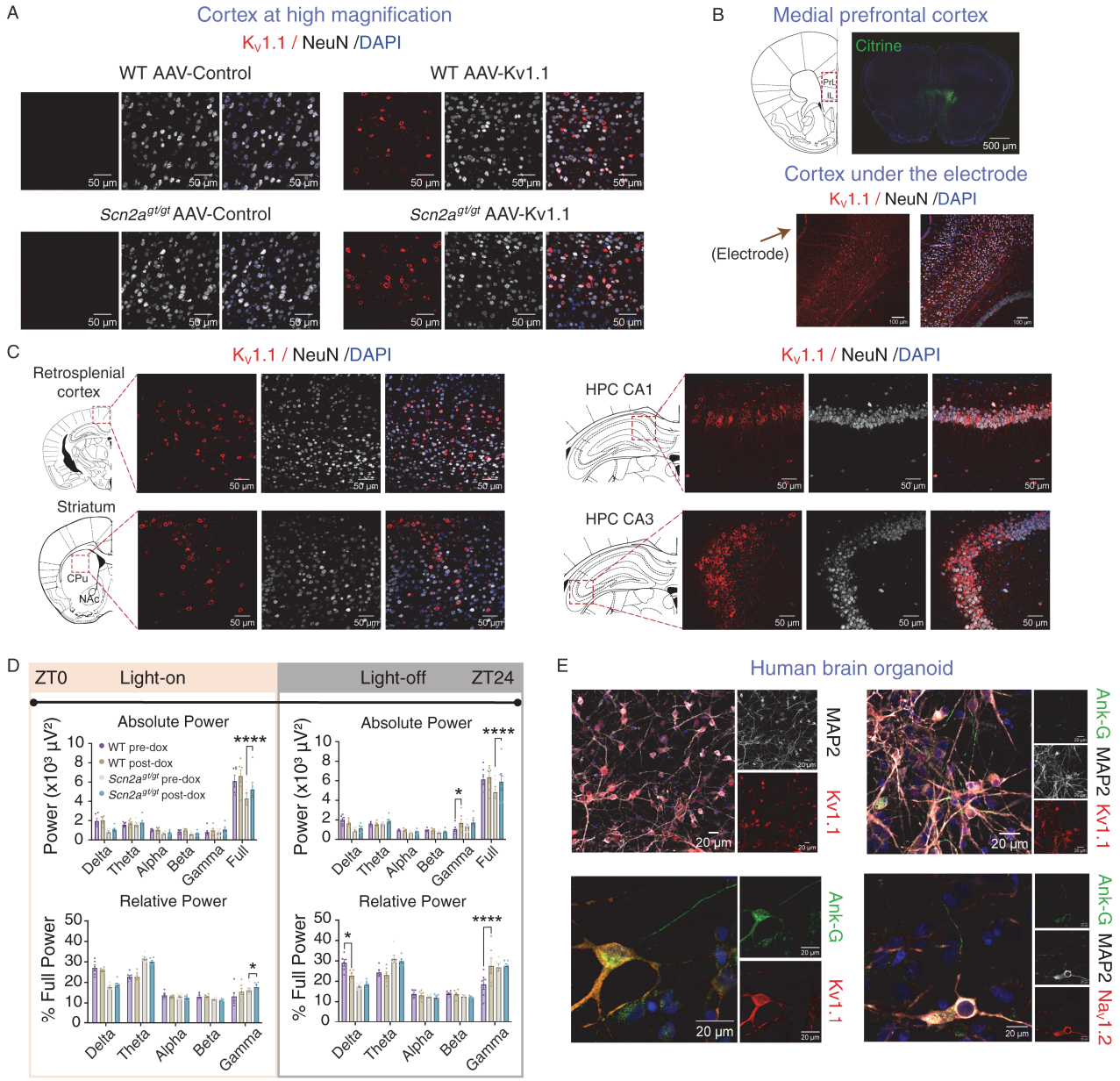
(A–F) Log2 fold changes in glutamate-, GABA-, myelin-, growth-, synaptic-, and calcium-related genes in D2J and B6 *Scn2a*$^{gt/gt}$ mice versus strain-matched WT controls.

(G) qPCR analysis of cortical *Cacng2* expression in D2J WT and *Scn2a*$^{gt/gt}$ mice (n = 6 per genotype). P values were calculated using an unpaired Student's t-test.

(H) Association between cortical *Cacng2* expression and spike-wave discharge (SWD) burden in D2J mice. P values were calculated using Spearman's correlation test.

Data are presented as mean ± SEM. **P* < 0.05; ***P* < 0.01; ****P* < 0.001; *****P* < 0.0001.

Supplemental Figure 9



Supplemental Figure 9. ICV *KCNA1* delivery produces widespread K_V1.1 expression and alters EEG spectra in D2J *Scn2a*$^{gt/gt}$ mice.

(A) High-magnification cortical IF images comparing AAV-control and AAV-*KCNA1*.

(B) AAV-control expression in medial prefrontal cortex (top) and K_V1.1 beneath the EEG electrode (bottom).

(C) K_V1.1 expression in retrosplenial cortex, striatum, and hippocampal CA1 and CA3.

(D) Absolute and relative EEG power pre-/post-doxycycline during light-on/off periods.

(E) Representative IF images of human K_V1.1 and Na_V1.2 in brain organoids cultured for >120 days.

Data are mean ± SEM. Two-way ANOVA with Šídák's multiple-comparisons test. **P* < 0.05; ***P* < 0.01; ****P* < 0.001; *****P* < 0.0001. Scale bars: A/C, 50 µm; B top, 500 µm; B bottom, 100 µm; E, 20 µm. Abbreviations: ICV, intracerebroventricular; AAV, adeno-associated virus; IF, immunofluorescence; EEG, electroencephalography.

Supplemental Table 1. Electrophysiological properties of cortical layer II/III pyramidal neurons at resting membrane potential (RMP).

Parameters	D2J WT	D2J *Scn2a*$^{gt/gt}$	*P*
Input resistance (MΩ)	73.7 ± 4.1	175.2 ± 14.5	<0.0001
RMP (mV)	−86.3 ± 0.3	−80.5 ± 1.0	<0.0001
Rheobase (pA)	689.3 ± 36.5	407.7 ± 22.1	<0.0001
AP threshold (mV)	−50.7 ± 0.9	−47.6 ± 0.6	0.0099
AP amplitude (mV)	117.9 ± 0.9	104.0 ± 1.6	<0.0001
AP fast AHP (mV)	−52.4 ± 1.2	−48.6 ± 0.5	0.0067
AP half-width (ms)	3.14 ± 0.12	3.34 ± 0.18	0.3686

Supplemental Table 2. Electrophysiological properties of cortical layer II/III pyramidal neurons at a fixed potential of -80 mV.

Parameters	D2J WT	D2J *Scn2a*$^{gt/gt}$	*P*
Input resistance (MΩ)	94.8 ± 6.2	171.7 ± 9.8	<0.0001
MP (mV)	−80.0	−80.0	—
Rheobase (pA)	597.9 ± 28.6	429.2 ± 21.9	<0.0001
AP threshold (mV)	−49.3 ± 0.8	−47.1 ± 0.6	0.0515
AP amplitude (mV)	110.5 ± 0.6	102.3 ± 0.9	<0.0001
AP fast AHP (mV)	−50.6 ± 0.9	−48.2 ± 0.5	0.0279
AP half-width (ms)	3.35 ± 0.10	3.44 ± 0.20	0.3937

Supplemental Table 3. Electrophysiological properties of striatal MSNs at the RMP.

Parameters	D2J WT	D2J *Scn2a*$^{gt/gt}$	*P*
Input resistance (MΩ)	62.2 ± 3.4	90.7 ± 4.7	<0.0001
RMP (mV)	−90.1 ± 0.3	−88.5 ± 0.5	0.0073
Rheobase (pA)	570.0 ± 28.3	511.5 ± 25.6	0.1404
AP threshold (mV)	−50.1 ± 0.8	−45.4 ± 0.8	0.0004
AP amplitude (mV)	118.6 ± 1.0	110.8 ± 0.9	<0.0001
AP fast AHP (mV)	−63.2 ± 0.9	−59.7 ± 1.0	0.0122
AP half-width (ms)	1.96 ± 0.05	2.30 ± 0.09	0.0022

Supplemental Table 4. Electrophysiological properties of striatal MSNs at a fixed potential of -80 mV.

Parameters	D2J WT	D2J *Scn2a*$^{gt/gt}$	*P*
Input resistance (MΩ)	104.1 ± 5.0	132.1 ± 4.4	0.0003
MP (mV)	−80.0	−80.0	—
Rheobase (pA)	431.4 ± 26.8	420.4 ± 20.8	0.7499
AP threshold (mV)	−49.1 ± 0.7	−45.5 ± 0.7	0.0017
AP amplitude (mV)	108.8 ± 0.8	102.7 ± 1.0	<0.0001
AP fast AHP (mV)	−62.4 ± 0.8	−58.8 ± 1.0	0.0102
AP half-width (ms)	1.90 ± 0.05	2.26 ± 0.10	0.0026

Data are presented as mean ± SEM. Statistical significance was determined by an unpaired two-tailed Student's t-test or Mann–Whitney test, as appropriate. *$P < 0.05$; **$P < 0.01$; ***$P < 0.001$; ****$P < 0.0001$.